Supporting information

Self-Assembly of Octapod-shaped Colloidal Nanocrystals into a Hexagonal Ballerina Network Embedded in a Thin Polymer Film

Milena P. Arciniegas[†], Mee. R. Kim[†§], Joost De Graaf[ξ], Rosaria Brescia[†], Sergio Marras[†], Karol Miszta[†], Marjolein Dijkstra[‡], René van Roij[¥], Liberato Manna[†]*

[†]Istituto Italiano di Tecnologia (IIT), via Morego 30, IT-16163 Genova, Italy.

[ξ]Institute for Computational Physics (ICP), University of Stuttgart, Allmandring 3, 70569 Stuttgart, Germany.

[‡]Soft Condensed Matter, Debye Institute for Nanomaterials Science, Utrecht University, Princetonplein 5, 3584 CC Utrecht, The Netherlands.

[¥]Institute for Theoretical Physics, Utrecht University, Princetonplein 5, 3584 CE Utrecht, The Netherlands.

1. Synthesis of octapods:

The synthesis procedure corresponds to those described in previous works by our group.[1, 2] In brief, colloidal CdSe/CdS nanocrystals were synthesized via a one-pot method: CdS pods were grown sequentially on the top of a CdSe seed pre-formed by rapid Cd^{2+}-cation exchange of $Cu_{2-x}Se$ nanocrystals in the same reaction flask.

Chemicals: Copper chloride (CuCl, 99.999%), tri-*n*-octylphosphine oxide (TOPO, 99%), *tri-n*-octylphosphine (TOP, 97%), and selenium (Se, 99.99%) were purchased from Strem Chemicals. *n*-Octadecylphosphonic acid (ODPA) and *n*-hexylphosphonic acid (HPA) were purchased from Polycarbon Industries. Propyl phosphonic acid (PPA), cadmium oxide (CdO, 99.99%), cadmium chloride ($CdCl_2$, 99.99 %), sulfur (S, 99.98%), oleylamine (70%), and 1-octadecene (90%) were purchased from Sigma-Aldrich. Anhydrous methanol and toluene were purchased from Carlo Erba reagents. All chemicals were used as received.

Synthesis of the $Cu_{2-x}Se$ Starting Seeds for Preparing Octapods: All synthesis procedures described here and in the next section were carried out using a standard Schlenk line. The synthesis of $Cu_{2-x}Se$ seeds followed the procedure previously reported.[3] 1 mmol of CuCl was mixed with 5 mL of oleylamine and 5 mL of 1-octadecene in a 50 mL three-neck flask. The mixture was heated under vacuum at 80 ^oC for 1 h and then heated up to 300 ^oC under N_2 flow. Meanwhile, a selenium precursor solution was prepared by dissolving 0.5 mmol of Se in 4 mL of oleylamine in a 25 mL three-neck flask. The mixture was put under vacuum at 130 ^oC for 1 h and heated to 230 ^oC under constant N_2 flow. When the Se was completely dissolved, the solution was cooled down to 180 ^oC for a fast injection by using a glass syringe equipped with a stainless steel needle into the above copper solution kept at 300 °C. After injection, the reaction was run at

300 °C for another 15 minutes. The flask was then cooled down to room temperature and the resulting black solution was quickly transferred into a N_2-filled vial for the sequent washing steps in a glove box under a N_2 atmosphere. $Cu_{2-x}Se$ nanocrystals were washed by repeated precipitation with methanol and re-dispersion in toluene, and the final seed nanocrystals dissolved in 3 mL of TOP. The concentrations of $Cu_{2-x}Se$ nanocrystals (with average size of 15 nm) in TOP was determined to be around $3 \cdot 10^{-6}$ M by inductively coupled plasma optical emission spectroscopy on digested solutions (with HCl/HNO_3 3:1 (v/v)).

Synthesis of CdSe/CdS Octapods: The synthesis procedure was according to those described in previous works by our group.[1, 2] Briefly, 0.060 g of CdO, 0.006 g $CdCl_2$, 0.305 g ODPA, 0.038 g HPA, 0.025 g PPA and 3.000 g of TOPO were loaded in a 25 mL three-neck flask and heated to 120 ^oC under vacuum for 1 h. The $CdCl_2$ amount is the critical factor to obtain very uniform and homogeneous octapod products and the ratio of the three phosphonic acids control the pod length of octapods. The temperature of the mixture was switched to 380 ^oC under N_2 flow and 2.6 mL of TOP was injected. In the glove box, 100 μL of a $3.0 \cdot 10^{-6}$ M solution of $Cu_{2-x}Se$ nanocrystals in TOP (corresponding, therefore, to $3.0 \cdot 10^{-10}$ moles of nanocrystals) was mixed with 0.5 g of TOP:S (previously prepared by dissolving 96 mg of S in 1 mL of TOP). The mixture was then injected rapidly into the reaction flask recovered to 380 °C. After the injection, the reaction was run for 10 min and then the reaction solution was cooled to room temperature. The resulting product was purified by washing with toluene and methanol, and finally dispersed in toluene (boiling point of 110.6 °C). Octapod-shaped nanocrystals presented a tip-to-tip length, *2L*, of 97 ± 4 nm and *Dp* of 12 ± 2 nm ($L/Dp \approx 4.0$), as determined by TEM analysis.

2. Film preparation and structure characterization:

Materials: Polymethyl methacrylate (PMMA) (M_w = 120.000 g/mol; M_w = 350.000 g/mol; T_g = 105 °C), toluene, acetone and isopropanol were purchased from Sigma-Aldrich.

Solutions of PMMA at 0.5, 1, and 5 % vol. in toluene were prepared and mixed with two concentrations of octapods (10^{-7} M and 10^{-8} M) in a 1:4 volume ratio. The mixed solutions were kept under vortex for a few minutes. The samples from both repeatedly-washed octapod solutions, with no polymer added, and octapod-polymer were prepared by drop casting and drying in air on the substrates. Two types of substrates were used: carbon-coated Cu grids for transmission electron microscopy (TEM) and SiO_2 wafers sputter-coated by a 10 nm-thick carbon film. The samples from the surfactant-rich octapod solution were prepared by drop casting of 5 μl of the solution on a SiO_2 wafer in a toluene-saturated atmosphere to allow slow drying.

Bright field (BF) transmission electron microscopy (TEM) analyses were conducted on a 100 kV JEOL JEM 1011 microscope. Energy-filtered TEM (EFTEM) images were acquired using a JEOL JEM-2200FS ultra-high resolution microscope, equipped with an in-column (Omega) energy filter and operated at 200 kV. The thickness of the PMMA layer embedding the hexagonal-ballerina assemblies was evaluated by computing the ratio between unfiltered BF-TEM and zero-loss filtered (EFTEM) images of octapod-empty regions (log-ratio method).[4] The inelastic mean free path of the 200 keV electrons through PMMA was calculated by assuming the PMMA molecular formula, $[CH_2C(CH_3)(CO_2CH_3)]_n$. A Tecnai G2 F20 TEM, operated at 200 kV acceleration voltages, was used to obtain single-tilt series of high angle annular dark field (HAADF)-scanning TEM (STEM) images of the octapod assemblies. The volume

reconstruction was done for the area in Figure S4 (see also movie SI2.avi) by weighted back-projection followed by 20 SIRT iterations, using the Tomoj plugin of ImageJ.[5, 6] The iso-surface rendering of the volume has been obtained using the UCSF Chimera package.[7] Scanning electron microscopy (JEOL JSM-7500FA) was conducted on both Carbon-coated film on TEM grids and SiO2 substrates with a 10 nm sputtered carbon coating. All substrates were cleaned before depositing the drops using 10 minutes of ultrasonic bath in acetone, distilled water and isopropanol. After cleaning they were carefully dried with pressurized air. A plasma reactor (Gambetti Tucano Multipurpose Plasma System) with an oxygen flow was used for the removal of the polymer from the substrates. The plasma exposure time was of 5 min at room temperature with a bias power level of 200 W.

After deposition, the thickness of the films was measured by an AMBiOS XP-2 Technology optical profilometer. Contact angles were determined by the sessile-drop method using OCA20 equipment - Dataphysics Instrument. One polar liquid, ultra pure MilliQ® - Millipore Corporation - was employed; 3 μl droplets were deposited at 1 ml/sec on the surfaces of the samples. The drop image was captured by the video camera and analysed using the SCA20 software. Both SiO_2 and SiO_2 with a sputtered carbon coating substrates were prepared under the same conditions and used as control material.

2. Supplementary figures and discussion:

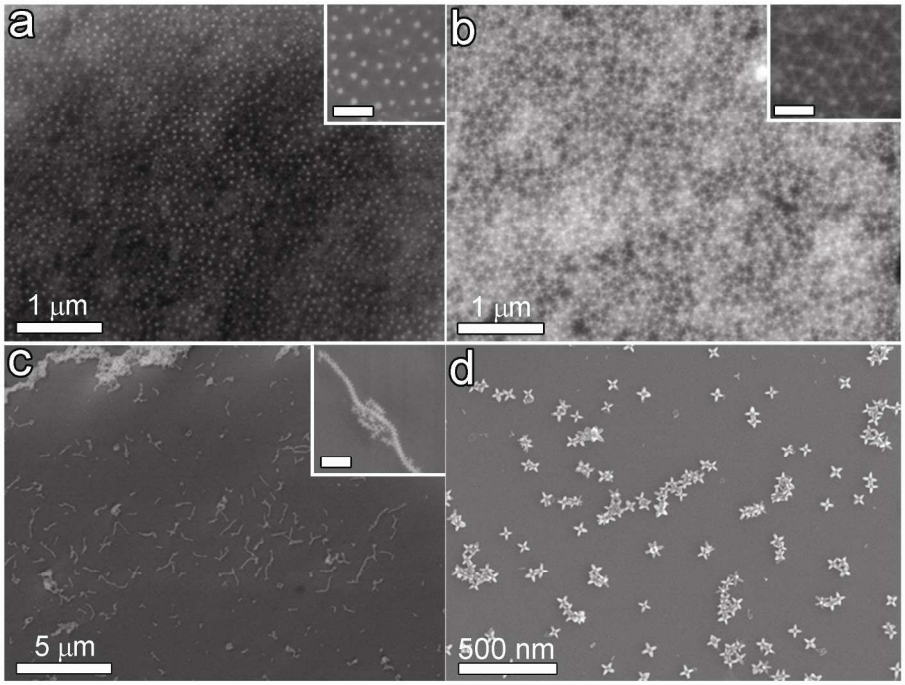

Figure S1. SEM images showing different configurations of octapods by varying the deposition variables. *a) Top view of the organic-rich solution of octapods, deposited on a SiO_2 substrate and subsequently allowed to dry slowly, showing the tips of the pods as bright white spots (SEI detector); the inset shows a closer view of the pods protruding from the organic film; scale bar: 100 nm. b) SEM image of the same zone revealing that seven pods of each octapod are embedded in the surfactant layer and confirming that six of these pods form the edges of an hexagonal structure with the surrounding octapods, as is further shown in the inset; scale bar: 100 nm (LABE detector). c) Formation of chain-like structures of octapods after slow evaporation of the purified solution. The inset image shows a closer view of a chain of interlocked octapods; scale bar: 200 nm. d) Octapods with four pods in contact with the substrate (presenting a cross-shape in a top view) after solvent evaporation in open air (fast evaporation) of a solution purified by four washing steps.*

Monitoring Octapod-Aggregation in PMMA Solution by Dynamic Light Scattering (DLS)

The formation of aggregates of octapods in solution by the addition of various concentrations of PMMA with two different molecular weights (M_w = 120.000 g/mol and M_w = 350.000 g/mol) was investigated by Dynamic Light Scattering (DLS) measurements. Figures S2a and S2b show the mean size distribution profiles for the fresh solution of octapods (200 μl of 10^{-7} M) in toluene before and after the addition of five different concentrations of PMMA (50 μl) of low and high molecular weight, respectively.

A narrow size distribution was observed from the fresh solution of octapods in toluene without PMMA. Clearly, agglomeration of octapods is produced in the solution by the addition of PMMA for both molecular weights, which is evidenced by the peaks being shifted towards larger sizes, but also by the broader intensity peaks for all the concentrations. This effect becomes stronger by the addition of PMMA with M_w = 120.000 g/mol at concentrations higher than 3%, for which the profiles present a bimodal size distribution. Additionally, it is evident that the increase in molecular weight induced a stronger aggregation in the solution from the change in the effective particle size from 92.3 ± 0.4 nm to 380 ± 20 nm (see Fig. S2b). Visual evidence of aggregation was also appreciated by changes in the transparency of the solutions prepared with the higher molecular weight PMMA (see inset in Fig. S2b for 1, 3, and 7% vol. from right to left); while the turbidity of the solutions containing PMMA with M_w = 120.000 g/mol was less evident (see inset in Fig. S2a).

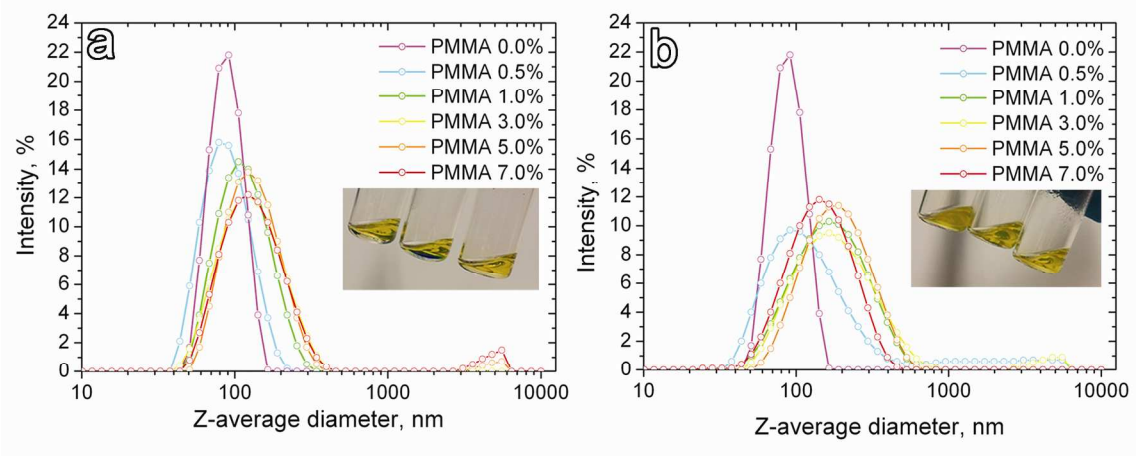

Figure S2. Monitoring octapod-aggregation in PMMA with different molecular weights. *Size-distribution profiles obtained by DLS shown the formation of octapod-aggregates by the addition of PMMA with (a) M_w = 120.000 g/mol and (b) M_w = 350.000 g/mol at different concentrations (% vol.). The inset images show the changes in transparency of the solutions after the addition of the polymer at 1, 3, and, 7 % vol. in toluene from right to left.*

Figure S3a shows the TEM images of the PMMA-based nanocomposites prepared at room temperature by solution casting, with a low concentration of octapods (10^{-8} M, 200 μl) in 50 μl of polymer with M_w = 120.000 g/mol at 0.5, 1.0, and 5.0 % vol. of polymer (M_w = 120.000 g/mol). Only a few octapods were observed to form short-range ordered structures. Figure S3b presents a collection of TEM images for different concentrations of PMMA with M_w = 350.000 g/mol, evidencing the formation of aggregates, the size of which decreased with the polymer content in toluene. The increase of the aggregate size for the lowest concentration of PMMA is attributed to the strong effect of polymer dewetting.

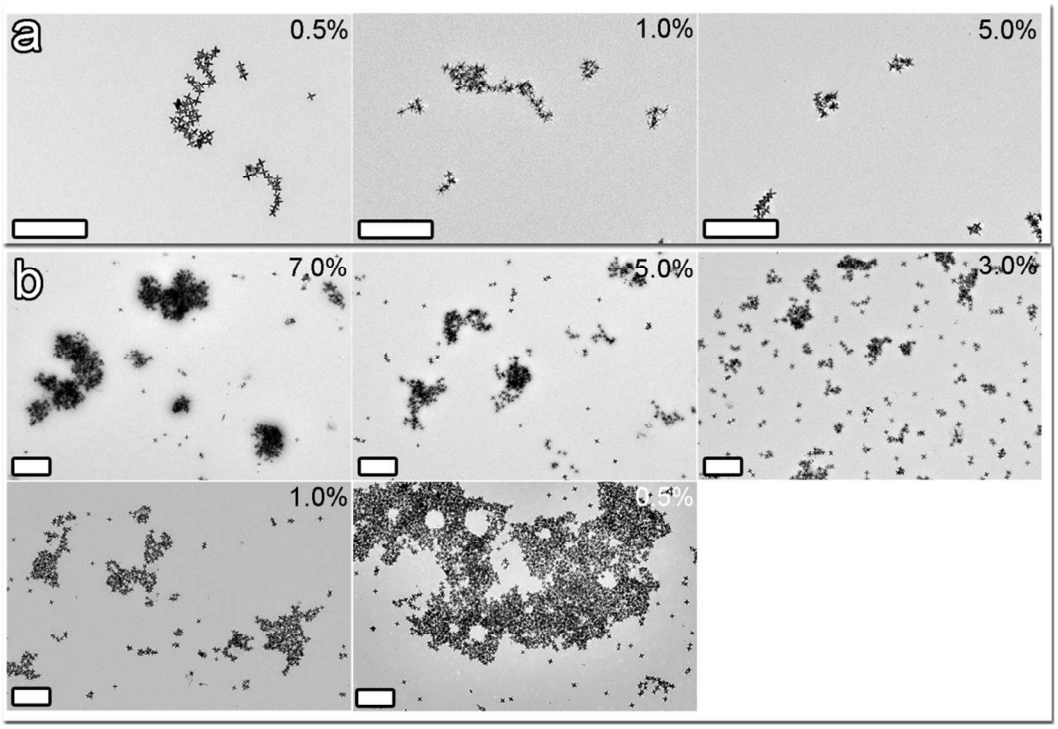

Figure S3. Octapod-aggregation in PMMA with higher molecular weight, M_w = 350.000 g/mol. *a) TEM images showing the lack of large ordered structures due to the low concentration of octapods, from left to right the PMMA concentration is 0.5, 1.0, and 5.0 % vol. b) TEM images of the PMMA-based nanocomposite revealing the presence of octapod aggregates of increasing size by decreasing the polymer concentration. Octapod concentration: 10^{-7} M, from left to right and top to bottom the PMMA concentration is 7.0, 5.0, 3.0, 1.0, and 0.5 % vol.*

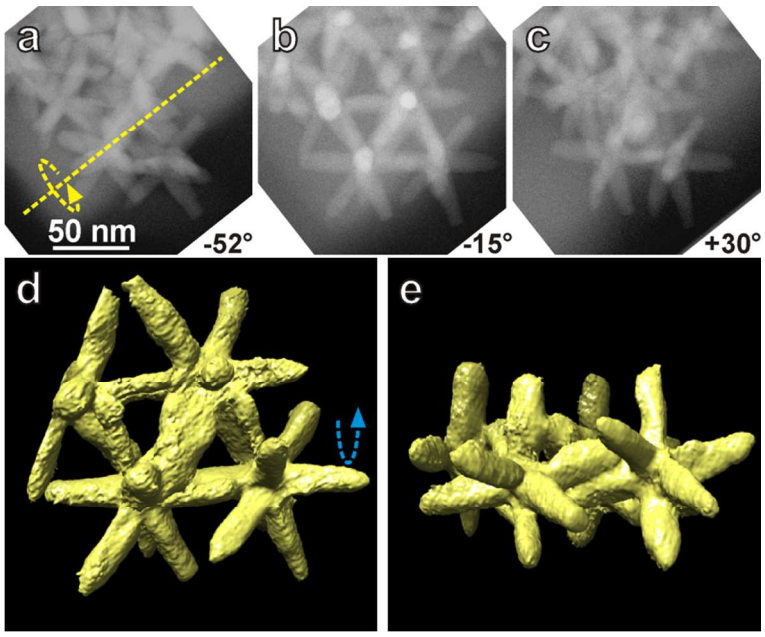

Figure S4. *a-c) HAADF-STEM images extracted from a single tilt series (from -60° to +70°) of a small group of octapods showing the ballerina orientation, with parallel pod-to-pod configuration (see supplementary movie SI2.avi for the complete tilt series). The tilt axis direction and rotation direction are indicated in a). d-e) Isosurface view of the volume reconstructed by electron tomography based on the same tilt series, viewed d) from top and e) from side, where the pod-to-pod parallel arrangement among neighboring particles is evident.*

3. Theoretical Investigation of the Wetting of Octapods:

In this section we consider the adsorption of a single octapod at a flat toluene/polymer-air interface using a theoretical model based on surface-tension arguments. We apply a model similar to that of P. Pieranski, who analyzed the strength of adsorption of spherical colloids at liquid-gas and liquid-liquid interfaces.[8] To describe the experimental system, we consider an octapod as the intersection of four spherocylinders which are oriented in the (±1,±1,1) directions and which are centered on the origin, similar to the model used in Refs. 9, 10. The tip-to-tip length of these spherocylinders is 2L, their diameter is D, thus the length of the cylindrical shaft is 2L - D, and their aspect ratio is given by L/D. In accordance with the experimental results we assumed an aspect ratio of L/D = 4.

We also considered a triangular-tessellation-based model similar to that of Ref. 11, again for a pod-to-diameter ratio of 4. The system is modeled as follows. In the spirit of the work by P. Pieranski, we consider the free energy of adsorption of a single octapod to see what its optimal (equilibrium) adsorption configuration is. The configuration of the particle can be described by four parameters: (i) the size of the particle, which is given by the multiplicative factor s; (ii) the height z of the particle with respect to the interface (as measured along the z-axis) – we locate the interface at $z = 0$ (xy-plane); (iii) rotation by the azimuthal angle ψ (around the z-axis); and (iv) rotation by the polar angle φ (around the y-axis). We assume that the octapod is first scaled by s, then rotated by ψ and subsequently by φ, and finally it is translated by z. Due to the symmetry properties of the octapod we can restrict ourselves to ψ in $[0,\pi/4]$ and φ in $[0,\pi/2]$. Even for this restricted range there are several instances of duplicate orientations, e.g., ψ in $[0,\pi/4]$ and $\varphi = 0$ gives essentially the same configuration as $\psi = 0$ and $\varphi = \pi/2$ for the same value of z. These duplicate configurations are taken into account via congruence in our analysis; see the

Supplementary Information to Ref. 12 for a similar approach. The octapod surface is assumed to have homogeneous surface properties and the two media, air and the toluene/polymer mixture are also assumed to be homogeneous. This is a significant simplification, since in the experiments the surface properties of the different facets are likely different and the media are presumably not homogeneous near the interface. In this system the free energy of adsorption F can be written as

Eq. 1: $$F(z, \psi, \varphi) = \gamma_{int}(A - S_{int}) + \gamma_{oa}S_{oa} + \gamma_{om}S_{om}$$

where γ_{int} is the liquid-air interfacial tension, A is the total surface area of the interface, S_{int} is the surface area excluded from the interface by the presence of the octapod, γ_{oa} is the surface tension between air and the octapod surface, S_{oa} is the total surface area of the octapod in contact with the air, γ_{om} is the surface tension between toluene/polymer mixture and the octapod surface, and S_{om} is the total surface area of the octapod in contact with the mixture. Note that we have made the dependence of S_{int}, S_{oa}, and S_{om} on (z, ψ, φ) implicit.

In this model, the microscopic degrees of freedom of the solvent molecules were integrated out to yield the surface tensions. We further assumed that the interface is not deformed by the presence of the particle: capillary deformation by gravity, electrostatic effects, or contact-angle requirements. These are strong simplifications, but there are too many unknowns regarding the experimental system to justify a more extended model. In this light, the results obtained in the next section should be seen as an indication of the possible behavior of an octapod at the interface, rather than a full theoretical description of the phenomenology in the experimental system.

To simplify the calculations we can reduce Eq. 1 by subtracting a constant contribution to the free energy of adsorption

Eq. 2: $$F'(z, \psi, \varphi) = F(z, \psi, \varphi) - [\gamma_{int}A + \gamma_{oa}(S_{oa} + S_{om}) + \gamma_{om}(S_{oa} + S_{om})];$$

Eq. 3: $$F'(z, \psi, \varphi) = (\gamma_{oa} - \gamma_{om})\, S_{oa} - \gamma_{int}S_{int};$$

Eq. 4: $$F'(z, \psi, \varphi) = \gamma_{int}[\cos\theta\, S_{oa} - S_{int}],$$

where we set the shifted free energy F' to zero when the colloid is completely immersed in the polymer/toluene mixture. In the last step (Eq. 4) we used Young's equation[13]

Eq. 5: $$\gamma_{oa} = \gamma_{int}\cos\theta + \gamma_{om},$$

with θ the contact angle corresponding to the octapod - air - polymer/toluene three-phase contact. Note that θ is determined by material properties, whereas ψ and φ are variables in our theory. Using the above equations we can now write the dimensionless free energy of adsorption as

Eq. 6: $$f(z, \psi, \varphi) = F'(z, \psi, \varphi)/(\gamma_{int}S) = [\cos\theta\, S_{oa} - S_{int}]/S,$$

with $S = S_{oa} + S_{om}$ the total surface area. Note that $f(z, \psi, \varphi)$ is independent of the size s of the particle. For a given θ, Eq. 6 gives rise to a three-dimensional (3D) free-energy landscape. This landscape was established by numerically determining the values of the various surface areas on a (z, ψ, φ) grid using the triangular-tessellation technique of Refs. 14, 15 we used 100 equidistantly spaced points in each direction. The thermodynamic equilibrium is assumed in the minimum of the free-energy landscape, i.e., the (z, ψ, φ) combination for which f has the lowest value. The density of grid points allows us to approach the actual minimum on our grid to within a sufficient level of precision to justify further analysis. Note that the presence of metastable

minima in the free energy of adsorption is not taken into consideration by analyzing the lowest free-energy value only.

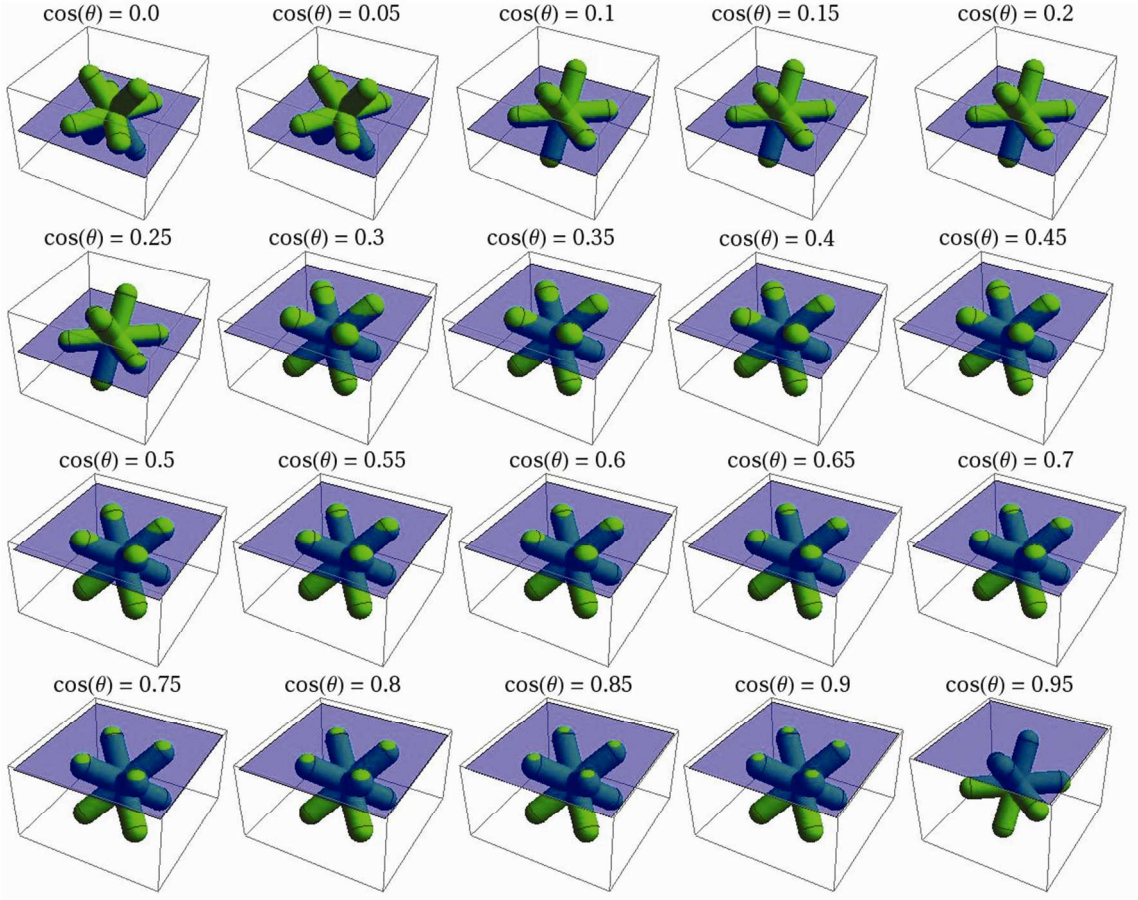

Figure S5. *Models for the optimal adsorption configuration of octapods (green spherocylinder model) partially immersed in a polymer monolayer as a function of the octapod wettability given by the cosine of the contact angle* $\cos\theta$*, which runs from 0.0 to 0.95. The interface is indicated by a transparent blue plane. Negative values of the contact angle result in configurations which are mirrored in the interface. Note that the configuration for the two lowest values of* $\cos\theta$ *are the same as the configurations for the other low-*$\cos\theta$ *values, just visualized from a different direction. Also note that the octapod is completely detached from the interface for* $\cos\theta = 0.95$*.*

An advantage of our model is that once the surface areas have been determined establishing $f(z, \psi, \varphi)$ for different values of θ in [0.0, 0.95] is simple. We did not consider negative values of θ since in our model a negative value of θ corresponds to mirroring the system in the interface. Our results, see Fig. S5, showed that the equilibrium orientations of the octapods (the results for the triangular model are not shown here) can be roughly divided into two categories: (I) four-arms lie flat on the interface and two stick out on either side and (II) the octapod rests on the interface with four tips slightly penetrating it (see Fig. S5). These configurations can be grouped under the two archetypical configurations given in the manuscript, since for the contact angles that we considered there are only slight variations with respect to these two. From Fig. S5 it follows that there is a sharp transition from configuration I to configuration II, with no intermediate states.

It is important to note that our results (and the conclusions we based on these) were obtained using a simple model for the adsorption of an octapod to an air-polymer/toluene interface. We leave a full investigation of the experimental phenomenology by theoretical or simulation means as an open problem for future study.

References

1. Kim, M. R.; Miszta, K.; Povia, M.; Brescia, R.; Christodoulou, S.; Prato, M.; Marras, S.; Manna, L. *ACS Nano* **2012,** 6, (12), 11088-11096.
2. Deka, S.; Miszta, K.; Dorfs, D.; Genovese, A.; Bertoni, G.; Manna, L. *Nano Lett.* **2010,** 10, (9), 3770-3776.
3. Korgel, B. A. *Nat. Mater.* **2010,** 9, (9), 701-703.
4. Egerton, R. F., *Electron Energy-Loss Spectroscopy in the Electron Microscope*. 3rd. ed.; Springer: New York, 2011.
5. Abramoff M.D., M. P. J., Ram Sunanda J. *Biophotonics international* **2004,** 11, (7), 36-42.
6. Cédric MessaoudiI, T. B., Carlos Oscar Sanchez Sorzano, Sergio Marco. *BMC Bioinformatics* **2007,** 8, 288-296.
7. Pettersen EF, G. T., Huang CC, Couch GS, Greenblatt DM, Meng EC, Ferrin TE. *J. Comput. Chem.* **2004,** 13, 1605-1612.
8. Pieranski, P. *Phys. Rev. Lett.* **1980,** 45, (7), 569-572.
9. Qi, W.; de Graaf, J.; Qiao, F.; Marras, S.; Manna, L.; Dijkstra, M. *J. Chem. Phys.* **2013,** 138, (15), 154504-13.
10. Qi, W.; Graaf, J. d.; Qiao, F.; Marras, S.; Manna, L.; Dijkstra, M. *Nano Lett.* **2012,** 12, (10), 5299-5303.
11. Miszta, K.; de Graaf, J.; Bertoni, G.; Dorfs, D.; Brescia, R.; Marras, S.; Ceseracciu, L.; Cingolani, R.; van Roij, R.; Dijkstra, M.; Manna, L. *Nat. Mater.* **2011,** 10, (11), 872-876.
12. Evers, W. H.; Goris, B.; Bals, S.; Casavola, M.; de Graaf, J.; Roij, R. v.; Dijkstra, M.; Vanmaekelbergh, D. *Nano Lett.* **2012,** 13, (6), 2317-2323.
13. Young, T. *Phil. Trans. R. Soc. London* **1805,** 95, 65-87.
14. de Graaf, J.; Dijkstra, M.; van Roij, R. *J. Chem. Phys.* **2010,** 132, (16), 164902.
15. de Graaf, J.; Dijkstra, M.; van Roij, R. *Phys. Rev. E.* **2009,** 80, (5 Pt 1), 051405-19.